Center Of Mass Motion Of The Cassini Spacecraft Due To Momentum Wheel Dumping

by

Marc A. Sengstacke, Ph.D.

California Institute Of Technology
Jet Propulsion Laboratory
301/220G
4800 Oak Grove Dr.
Pasadena, Calif., 91109-8099
(818) 354-0371

February, 1994

Abstract

The Cassini spacecraft is scheduled for launch to Saturn in October of 1997. During portions of the mission, momentum wheels will be used for attitude control. When the angular momentum of any wheel reaches a specified maximum, it will be necessary to reduce the angular momentum. This will be done by having the spacecraft exert a torque on the wheel. This in turn will generate a torque by the wheel on the spacecraft that will cause the spacecraft to undesirably spin unless countered by an opposing torque. Therefore, during momentum wheel dumping, attitude control thrusters will be used to provide this opposing torque so that the spacecraft maintains an inertially fixed rotational state. However, since some of the thrusters are uncoupled, the spacecraft center of mass velocity, $\Delta\vec{\mathbf{V}}_{cm}$, will change. This change will have a significant impact on the spacecraft trajectory, orbit determination and maneuver design and must therefore be understood.

ROTRAN is a computer simulation package developed by this author for *JPL* navigation for the purpose of generating the $\Delta\vec{\mathbf{V}}_{cm}$ resulting from attitude maneuvers. *ROTRA* N will be used here to study the $\Delta\mathbf{V}_{cm}$ resulting from momentum wheel dumping.

Given the studied thruster configurations, it will be shown that $\Delta\vec{\mathbf{V}}_{cm}$ is approximately independent of the body fixed z component of the total torque applied to the wheels and approximately linearly related to the xy components. Separate linear coefficients can be applied in each quadrant of the xy plane. The approximations are valid to witbin about $\pm 5\%$ in most cases.

Contents

1 Introduction

The goal of project Cassini is to extensively study the Saturnian planetary system. The Cassini spacecraft is scheduled for launch in October of 1997 with an arrival at Saturn in June of 2004.

The Cassini spacecraft attitude will be controlled by a combination of momentum wheels and thrusters. Momentum wheels are speed controlled wheels on board the spacecraft. By applying appropriate torques to speed up or slow down the wheels, opposing torques on the remainder of the spacecraft will cause a counter rotation, the proper use of which will lead to the desired new attitude.

At various times, combinations of the wheels will reach maximum spin rates, at which point the spin rater must reduced. This is called momentum wheel dumping and is accomplished by applying an appropriate torque to the wheel. However, just as in attitude control, the spacecraft will counter rotate unless a counter torque is applied. This counter rotation is undesirable. Therefore, a counter torque is provided by thrusters such that the spacecraft rotational state remains inertially fixed (to a first approximation) during the dump. The thrusters are controlled by the Cassini Attitude and Articulation Control System *(AA CS [I], [2]).*

The thruster firings during dumping generate a center of mass velocity change, $\Delta\vec{\mathbf{V}}_{cm}$, that will have a significant impact on the spacecraft trajectory, orbit determination and maneuver design. Therefore, this change must be understood. For this and other reasons, the computer simulation package *ROTRAN was* designed and developed by this author for the purpose of studying the $\Delta\vec{\mathbf{V}}_{cm}$ resulting from general attitude maneuvers. *ROTRAN* will be used here to study the $\Delta\vec{\mathbf{V}}_{cm}$ resulting from thrusters firings used to provide counter torques during momentum wheel dumping.

It will be shown that $\Delta\vec{\mathbf{V}}_{cm}$, under conditions studied here, is independent of the total z component of the torque on all the wheels and linearly related to the x and y components. Different, linear coefficients apply in each of the four quadrants of the xy plane.

2 Dynamics Of A Momentum Wheel Dump

2.1 The Torque On The Wheels

A picture of the Cassini spacecraft is shown in Fig. (1). The spacecraft is divided into two disjoint sets. One set consists of the momentum wheels only. The other consists of the remainder of the spacecraft, called the *basebody*. $[S]$ and $[B]$ are parallel basebody fixed frames. The origin of $[B]$ is at the basebody center of mass while the origin of [S] is general.

The axis of rotation of each wheel is assumed fixed relative to [B]. Each wheel is assumed symmetric about its axis of rotation.

Under the above and other symmetry conditions, the torque exerted by the basebody on a given wheel is opposite the torque exerted, by the wheel on the basebody. Define $\vec{\mathbf{N}}_{wb}$ as the total torque on all wheels due to the basebody. The torque on the basebody due to all wheels is therefore $\vec{\mathbf{N}}_{bw} = -\vec{\mathbf{N}}_{wb}$. The total torque on the basebody, $\vec{\mathbf{N}}_b$, is assumed to consist of torques from the wheels and thrusters only $(\vec{\mathbf{N}}_t)$. It is this torque that is used in the Euler equations for the basebody to determine its attitude and attitude rate.

$$\vec{\mathbf{N}}_b = \vec{\mathbf{N}}_t + \vec{\mathbf{N}}_{bw} \qquad 1)$$

$$= \vec{\mathbf{N}}_t - \vec{\mathbf{N}}_{wb} \qquad 2)$$

Assuming that only the basebody exerts a torque on any wheel, the "6" will be dropped in $\vec{N}_{wb}$ and written $\vec{N}_w$.

The following is assumed for an actual wheel dump. First of all, the dump begins with $[B]$ having O angular velocity relative to inertial space. The torque on wheel i, $\vec{N}_{wi}$, is commanded to remain fixed relative to the basebody for a given time ΔT_{wi}. The torque will point along the axis of rotation, In this study, ΔT_{wi} is the same for all wheels, ΔT_w. Therefore, the total torque on all the wheels is constant at $\vec{N}_w$ during ΔT_w and zero otherwise. For each value of $\vec{N}_w$, a $\Delta \vec{V}_{cm}$ will result as the basebody attempts to remain inertially fixed during t he time ΔT_w. Characterizing the dependence of $\Delta \vec{V}_{cm}$ on $\vec{N}_w$ under the above conditions is the primary goal of this study.

Note that all that maters is the total torque $\vec{N}_w$, regardless of how the wheels are oriented relative to $[B]$. Therefore, the remainder of this study will involve varying $\vec{N}_w$ without consideration of wheel orientation.

2.2 Predicted Velocity Changes

Fig. (2) shows the positions of the *AACS* thrusters in two configurations relative to [S] (Note that Fig. (2) is upside down relative to Fig. (l), for the high gain antenna points in the $-z$ direction). In the case of Fig. (2a), turns about the x axis are accomplished using either thruster pair (1, 2) (for $-x$ turns) or *(3,4)* (for $+x$ turns). Since each member of the pair points in the –z direction, corrections about the x axis will generate a $-z$ component of $\Delta \vec{V}_{cm}$. Correspondingly, turns about the y axis are accomplished using either thruster pair (1, 4) (for $+y$ turns) or (2, 3) (for –y turns). Again, corrections about the y axis generate changes in $\Delta \vec{V}_{cm}$ along $-z$. By contrast, rotations about the z axis are accomplished using either thruster pair (6, 7) (for $+z$ t urns) or (5,8) (for $-z$ turns). These pairs are coupled and therefore lead to no CM velocity change. If $\vec{N}_w$ has a 2 component, $N_{wz} > 0$, then $[B]$ will include in its motion a turn about the z axis, Once the deadband is reached, thruster pair (6, 7) or (5, 8) will fire to correct tile z error. Since these pairs are coupled, they have no effect on $\Delta \vec{V}_{cm}$. The first prediction is that $\Delta \vec{V}_{cm}$ is independent of the z component of $\vec{N}_w$ given an x and y component.

The x component N_{wx} will generate an x axis turn of $[B]$. Again, when the deadband is reached, thruster pair (1, 2) or (3,4) will fire accordingly. In either case, as onc can see from Fig. (2a), the resultant $\Delta \vec{V}_{cm}$ will be in the $-z$ direction. Note that the basebody will cycle through hitting the deadband followed by thrusters returning the state to within the deadband. This will take place throughout ΔT_w. Note that the larger the torque, the sooner the deadband is reached in each cycle, and the longer the thrusters fire throughout AT.,. Assuming a linear relationship between the total firing time and N_{wx}, then, using Newton's laws, V_{cmz} will linearly increase in magnitude in the $-z$ direction with increasing magnitude in N_{wx}. $V_{cmz} = O$ for $N_{wx} = 0$.

Now consider the case where N_{wy} is fixed and nonzero and where N_{wx} is allowed to vary. The constant N_{wy} will add to the amount of time that the thrusters fire during ΔT_w. It is assumed that all this will do is add an offset to the V_{cmz} vs N_{wx} curve in the $-z$ direction. This assumption is valid if there are not too many sample periods where x and y corrections are simultaneously needed (otherwise only one common thruster from two pairs will fire [1]).

Finally, the relationship between x and y can be reversed in the above argument. This should make clear the $3D$ plots of V_{cmz} Vs (H_{wx}, H_{wy}) (see Eqs. (3) and (5)) in Figs, (4) and (5) which were generated using *ROTRAN*.

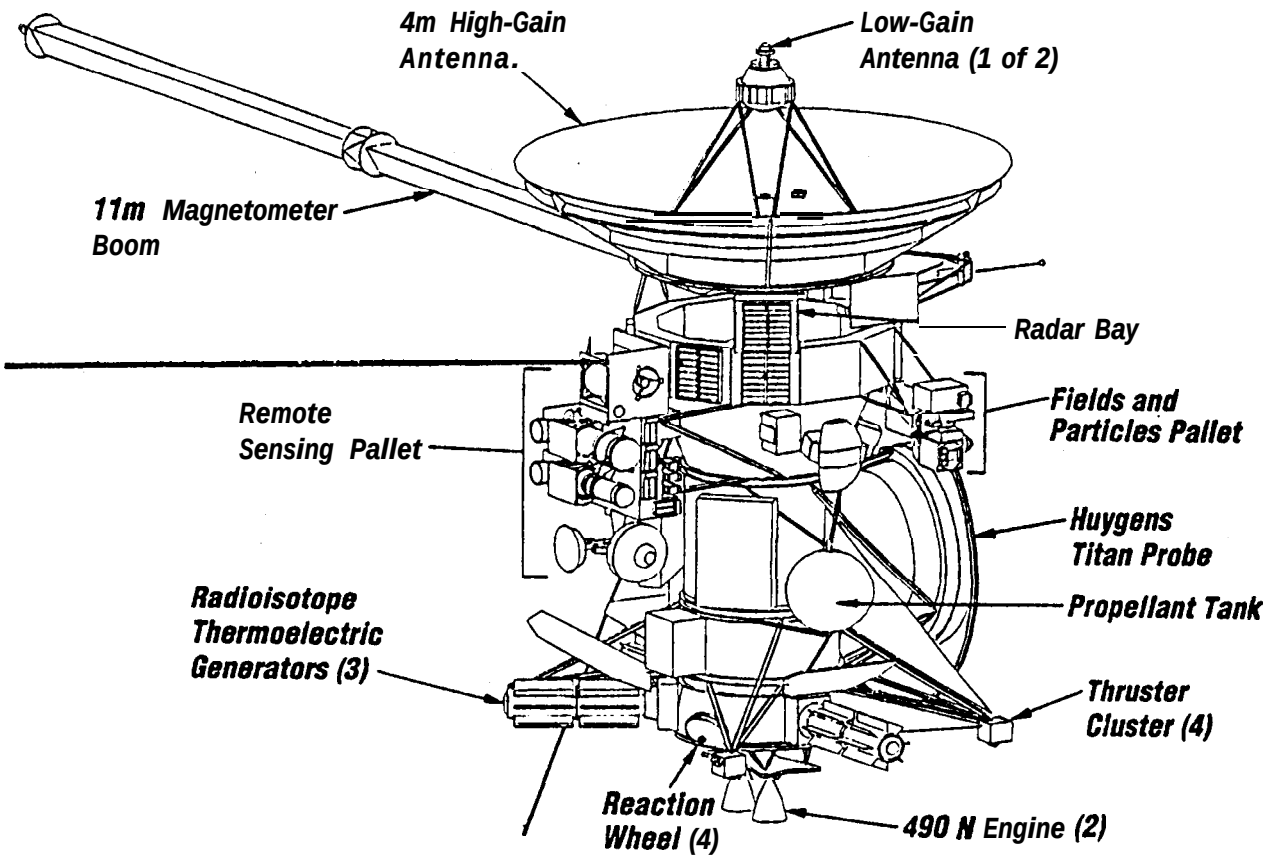

Figure 1: The Cassini Spacecraft

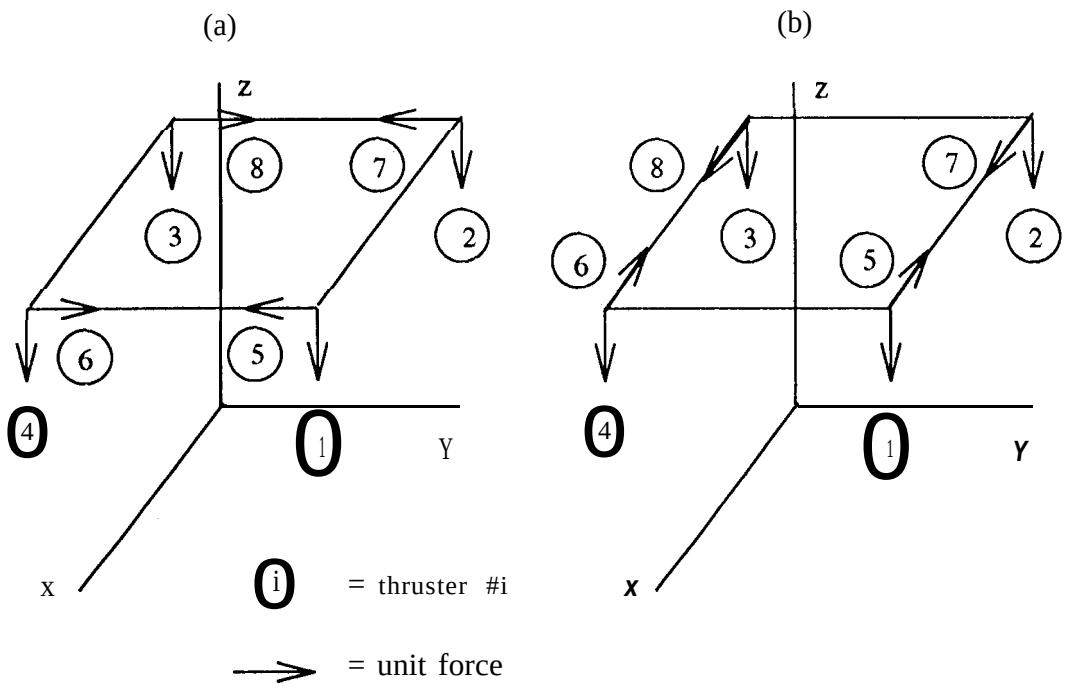

Figure 2: Two thruster configurations in [S]

3 Simulation Results

3.1 Overview

The first step will be to establish the independence between $\Delta\vec{\mathbf{V}}_{cm}$ and N_{wz}. Given, this the variation of $\Delta\dot{\mathbf{V}}_{cm}$ with the xy component, of the torque, $(N_{wx}, N_{wy}$,will be studied with N_{wz} conveniently set to O. Table (1) is a list of parameters that arc constant for all cases (thruster coordinates are taken from reference [3]).

3.2 The Relationship Between $\Delta\vec{\mathbf{V}}_{cm}$ And N_{wz}

3.2,1 Case Description

In this case, (N_{wx}, N_{wy}) 'are held fixed while N, is allowed to vary, as shown in Fig. (3). Eight settings of (N_{wx}, N_{wy}) are used. They include four cases where the xy component is along $(\pm x, \pm y)$ and four cases where the xy component is along the 45° diagonal.

This case will use the thruster configuration in Fig. (2 b). However, the thrusters used for z axis turns are coupled as in the configuration in Fig, (2a). Therefore, the generated $\Delta\vec{\mathbf{V}}_{cm}$ should be independent of N_{wz} for the same reasons discussed in Section (2.2). However, the total $\Delta\vec{\mathbf{V}}_{cm}$ is not all in the $-z$ direction because x facing thrusters are used to generate y axis turns, Therefore, $\Delta\dot{\mathbf{V}}_{cm}$ will in general have an x and z component. Nevertheless, if independence between $\Delta\mathbf{V}_{cm}$ and N_{wz} is found for the configuration in Fig. (2 b), then independence will also be assumed for the configuration in Fig. (2a).

Parameters for this case are in Tables (1) and (2).

Parameter	Value
Control law.	BANG/BANG
Dead band (radians, (XYZ)).	$2 * 10^{-3}$
$AACS$ sample time Δt_s (sec).	0.125
$ROTRAN$ sample time Δt_r (sec).	0.025
BANG/BANG time constant (seconds (XYZ)).	3
Thruster force magnitude (N).	0.51
Thruster on time in each AACS sample period.	Δt_s
Momentum wheel on time ΔT_w (secs).	100

Thruster	XY coordinates in [S] (meters) (all thrusters have a z coordinate off 3 meters)	
1	1.26	1.58
2	–1.25	1.58
3	–1.26	–1.58
4	1.25	–1.58
5	1.26	1.58
6	1.25	–1.58
7	–1.25	1.58
8	–1.26	–1.58

Table 1: Parameters constant for all cases

Parameter	Value
Basebody center of mass in [S] (meters)	(-0.05 S287, 0.020037, 1.266)
Spacecraft mass (including wheels) (Kg)	$2.425 * 10^3$
Basebody inertia tensor in [B], xx, xy, yy, xz, yz and $zz (KgM^2)$	(5939.3, -86.469,4997.3,-13.04, 101.94,2937.7)

Thruster	Unit Force Direction
1	$-Z$
2	$-Z$
3	$-Z$
4	$-Z$
5	$-X$
6	$-X$
7	$+X$
8	$+X$

Table 2: Additional parameters constant for study of $\Delta\vec{\mathbf{V}}_{cm}$ vs N_{wz}

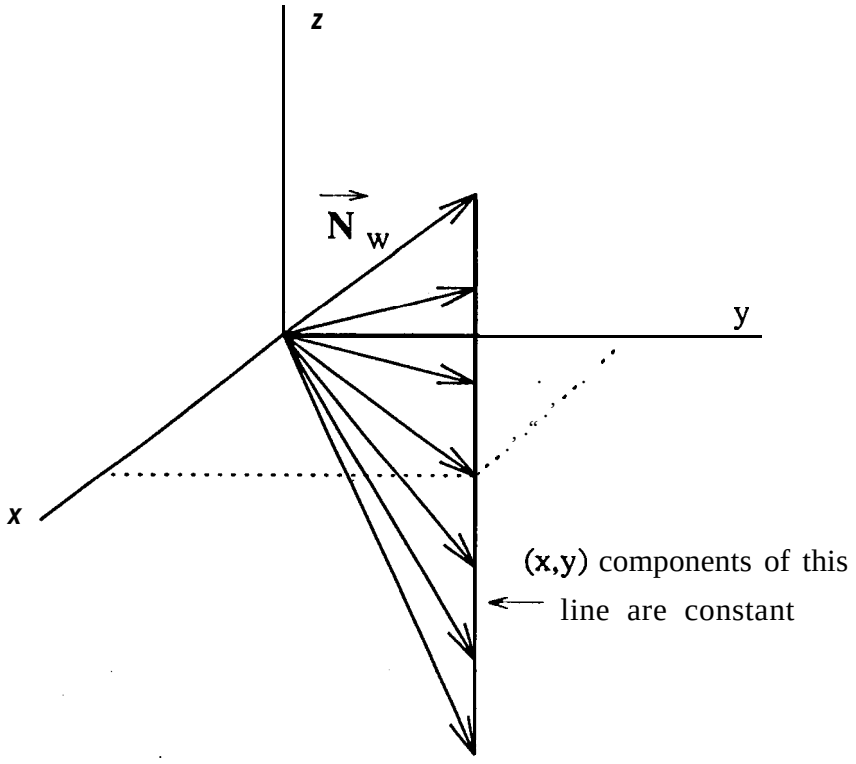

Figure 3: Geometry for determining the relationship between $\Delta\vec{\mathbf{V}}_{cm}$ and N_{wz}

(N_{wx}, N_{wy}) = (4,0)* $10^{-2}NM$

Test	$N_{wz}(NM)$	Final velocity in [B] (m/sec)		
1	$0.0 * 10^{-2}$	$-5.303551445040552 * 10^{-5}$	$-11.874931066234415 * 10^{-6}$	$-1.208768437155959 * 10^{-3}$
2	2.0*lo-^{2}	$-5.306887448033524 * 10^{-5}$	$-1.856845411210250 * 10^{-6}$	$-1.208768535322538 * 10^{-3}$
3	4.0*lo-^{2}	$-5.308125061097936 * 10^{-5}$	$-1.930903122105568 * 10^{-6}$	$-1.208768353187503 * 10^{-3}$
4	-2.0 * lo-^{2}	$-5.299126078190660 * 10^{-5}$	$-2.116673667893593 * 10^{-6}$	$-1.208768608607155 * 10^{-3}$
5	$-4.0 * 10^{-2}$	$-5.299226471860074 * 10^{-5}$	$-1.877793244193318 * 10^{-6}$	$-1.208768214174606 * 10^{-3}$

'l'able 3: Best case result in study of $\Delta\vec{\mathbf{V}}_{cm}$ vs $\vec{\mathbf{N}}_{wz}$

(N_{wx}, N_{wy}) = (2.828, -2.828)$*10^{-2}NM$

Test	$N_{wz}(NM)$.	Final velocity in [B] (m/sec)		
1	–4.O*1O-2	$-6.848881496764135 * 10^{-4}$	$-2.677624971668803 * 10^{-7}$	$-7.347916787743196 * 10^{-4}$
2	–3.0* 10-2	$-6.848878632807274 * 10^{-4}$	$-1.266704567411953222 * 10^{-7}$	$-7.347924837773330 * 10^{-4}$
3	$-2.0 * 10^{-2}$	$-6.848891400792487 * 10^{-4}$	$-2.652081976698279 * 10^{-7}$	$-7.347910613812493 * 10^{-4}$
4	$-1.0 * 10^{-2}$	$-6.848897620310880 * 10^{-4}$	$-2.487113990384675 * 10^{-7}$	$-7.347910705689384 * 10^{-4}$
5	O. O*1O-2	$-6.848928345360353 * 10^{-4}$	$-1.123526134022569611 * 10^{-7}$	$-7.347920848712862 * 10^{-4}$
6	I. O*1O-2	$-6.848938827350818 * 10^{-4}$	$-2.812485079234042 * 10^{-7}$	$-7.347931712516827 * 10^{-4}$
7	$2.0 * 10^{-2}$	$-6.848946520517795 * 10^{-4}$	$-1.382339797201592 * 10^{-7}$	$-7.347924486628747 * 10^{-4}$
8	$3.0 * 10^{-2}$	$-6.848939578274178 * 10^{-4}$	$-1.146926235960155 * 10^{-7}$	$-7.347925080772423 * 10^{-4}$
9	$4.0 * 10^{-2}$	–6.586082204541109 *10-4	- 1.605614433763609*10-(	-7.348432765430558* 10^{-4}

Table 4: Worst case result in study of $\Delta\vec{\mathbf{V}}_{cm}$ vs $\vec{\mathbf{N}}_{wz}$

3.2.2 Results

Tables (3) and (4) are respectively best and worst case results. In Table (3), the xy torque is along the $+x$ axis. In this case, -z facing thrusters are used (Fig.(2b)). Therefore, the dominant velocity component is in the -z direction. This shows in the table since the x and y velocity components are two to three orders of magnitude below the z component. These components are therefore ignored. Note also that the z component has no variation thru the first seven significant digits. In Table (4), the xy torque is in the $(+x, -y)$ direction, In this case, $-x$ and -z facing thrusters are used leading to dominant velocity components in the same directions, Again, this occurs since the y component is better than three orders of magnitude less. The x component has a maximum variation of about, 0.0263 * 10^{-3} m/see or approximately 4% of the minimum value. Therefore, it is concluded that $\Delta\vec{\mathbf{V}}_{cm}$ is independent of N_{wz} to within a 4% variation in the worst case,

3.3 The Relationship Between $\Delta\vec{\mathbf{V}}_{cm}$ And (N_{wx}, N_{wy})

3.3.1 Case Description

In this case, $\Delta\vec{\mathbf{V}}_{cm}$ is assumed independent of N_{wz}. Therefore, N_{wz} is set to O. (N_{wx}, N_{wy}) is varied in discrete steps over a square in the xy plane centered at the origin. In other words,

$$(N_{wx}, N_{wy}) = (n_x, n_y)\Delta N \tag{3}$$

Thruster directions used for BOM and EOM conditions

Thruster	Unit Force Direction
1	$-Z$
2	$-Z$
3	$-Z$
4	$-Z$
5	$-Y$
6	$+Y$
7	$-Y$
8	$+Y$

Mass properties for BOM and EOM conditions

Parameter	BOM Value	EOM Value
Spacecraft mass (including wheels) (Kg)	5222.2	2019.2
Basebody center of mass in [S] (meters)	$(-0.03, -0.03, 1.38)$	$(0.15, 0.03, 1.16)$
Basebody inertia tensor in [B], top row = (xx, xy, yy), bottom row = $(xz, yz, zz)(KgM^2)$	7625.0 −85.2 8020.6 137.4 −61.2 3394.8	5636.5 −80.5 4727.0 −34.6 66.6 2909.5

Table 5: Parameters constant for *BOM* and *EOM cases*

where $-n_o \leq n_x, n_y \leq n_o, n_o$ = 10 and AN = 0.01 NM. For each (N_{wx}, N_{wy}), a $\Delta\vec{\mathbf{V}}_{cm}$ is generated.

Given the constant wheel on time ΔT_w (Table (1)), one can define the following angular momenta.

$$(H_{wx},\ \text{H.},) = \Delta T_w(N_{wx}, N_{wy}) \tag{4}$$

'l'his leads to the following rewrite of Eq. (3) where $\Delta H = \Delta T_w \Delta N$.

$$(H_{wx}, H_{wy}) = (n_x, n_y)\Delta H \tag{5}$$

From Table (l), ΔH = I. ONMS.

The above will be done in two subcases. One for beginning of mission (BOM) conditions. The other for end of mission (EOM) conditions. These two subcases have been chosen because they provide an envelope (of some kind) surrounding most other situations.

Parameters constant for *BOM* and EOM conditions are in Tables (1) and (5). Mass properties (total mass, center of mass and inertia tensor) are taken from reference [3], In these two subcases, the thruster configuration of Fig. (2a) will be used. Therefore, the velocity change will be in the $-z$ direction, as described in Section (2.2).

3.3,2 Results

Three dimensional contour plots of V_z *vs* (H_{wx}, H_{wy}) are shown in Figs.(4) and (5) respectively for BOM and EOM cases. These plots were generated using raw data as outlined by Eq. (5). Note that the plots have the general characteristic discussed in Section (2.2). Also note the larger velocity in Fig. (5). This is due to the reduced mass in this case (Table (5)). Figs. (6) and (7) are $2D$ contour plots respectively for *BOM* and EOM conditions. From Figs. (4) to (7), it should be clear that for

each quadrant of (N_{wx}, N_{wy}), the $3D$ contour plots of V_z vs (N_x, N_y) approximately form a plane. Thus the following holds with in general different coefficients in each quadrant and where $i = 1 \cdots 4$ respectively corresponds to quadrants $(+x, +y), (+x, -y), (-x, -y)$ and (–r, $+y$).

$$V_z \approx C_{ix} H_{wx} + C_{iy} H_{wy} \tag{6}$$

The coefficients $C_i = (C_{ix}, C_{iy})^t$ are found using a pseudo-inverse technique. First, assume that n of the data points in Eq. (3) are in quadrant i. Then one has the following.

$$\begin{aligned} V_{1z} &\approx C_{ix} H_{w1x} + C_{iy} H_{w1y} \\ V_{2z} &\approx C_{ix} H_{w2x} + C_{iy} H_{w2y} \\ \cdots \quad &\cdots \quad \cdots \\ V_{nz} &\approx C_{ix} H_{wnx} + C_{iy} H_{wny} \end{aligned} \tag{7}$$

V is a column matrix such that $\mathbf{V}_m = V_{mz}$. Also define the $(n \times 2)$ matrix $\mathbf{H}_{wxy}$ such that its mth row is (H_{wmx}, H_{wmy}). This leads to the next equation.

$$\mathbf{V} \approx \mathbf{H}_{wxy} \mathbf{C_i} \tag{8}$$

Now multiply the above by the transpose, $\mathbf{H}^t_{wxy}$.

$$\mathbf{H}^t_{wxy} \mathbf{V} \approx \mathbf{H}^t_{wxy} \mathbf{H}_{wxy} \mathbf{C_i} \tag{9}$$

The matrix $\mathbf{H}^t_{wxy} \mathbf{H}_{wxy}$ is square. If it has an inverse, then the next equation results when it multiplies the above equation.

$$\mathbf{C_i} \approx \left(\mathbf{H}^t_{wxy} \mathbf{H}_{wxy}\right)^{-1} \mathbf{H}^t_{wxy} \mathbf{V} \tag{lo}$$

'I'his equation will be evaluated for each quadrant

Results for each quadrant for BOM and EOM conditions are shown in Figs. (8) thru (15). Each figure contains three contour plots. They include one generated from $ROTRAN$ simulations, one using the linear approximation of Eq. *(6)* and one of the percentage difference between the previous two.

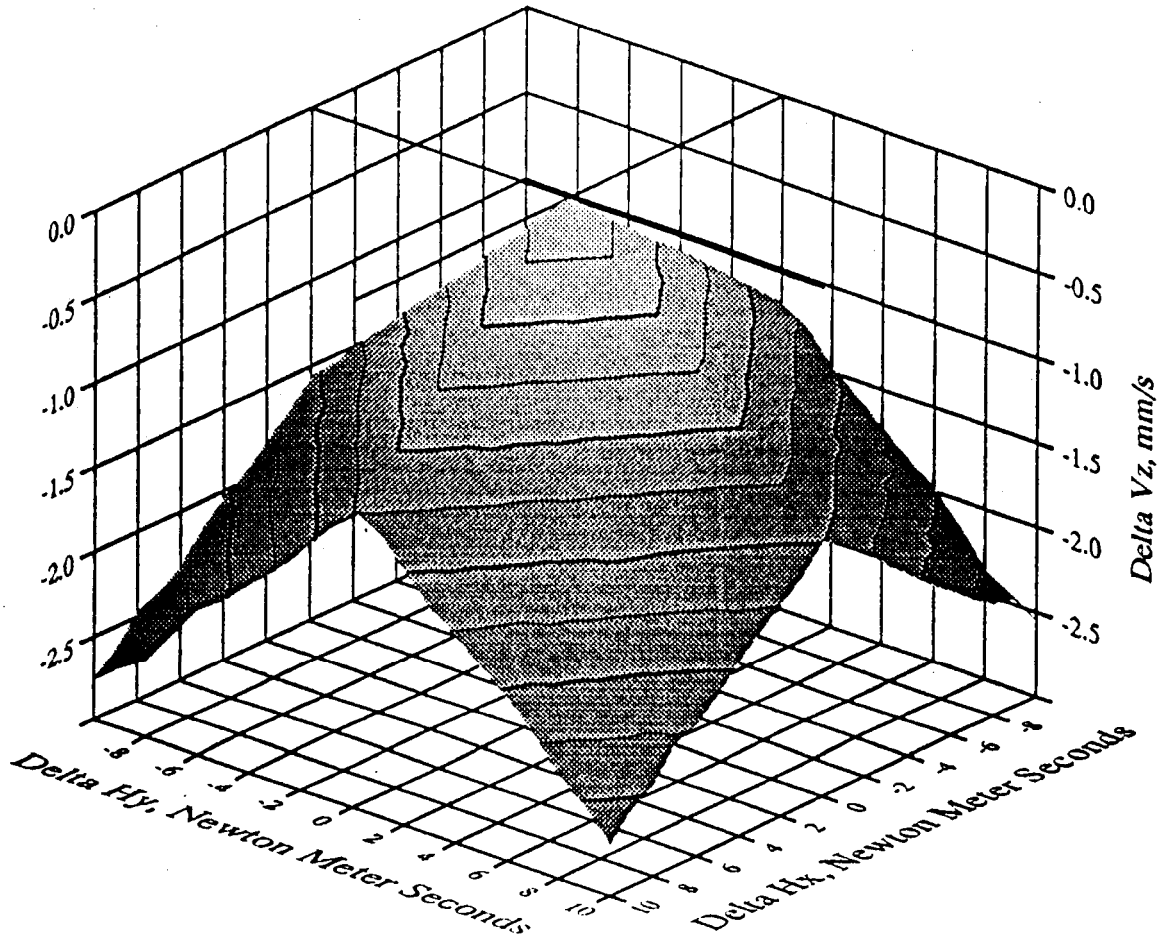

Figure 4: 3D contour plots of V_z versus (H_{wx}, H_{wy}) for BOM conditions

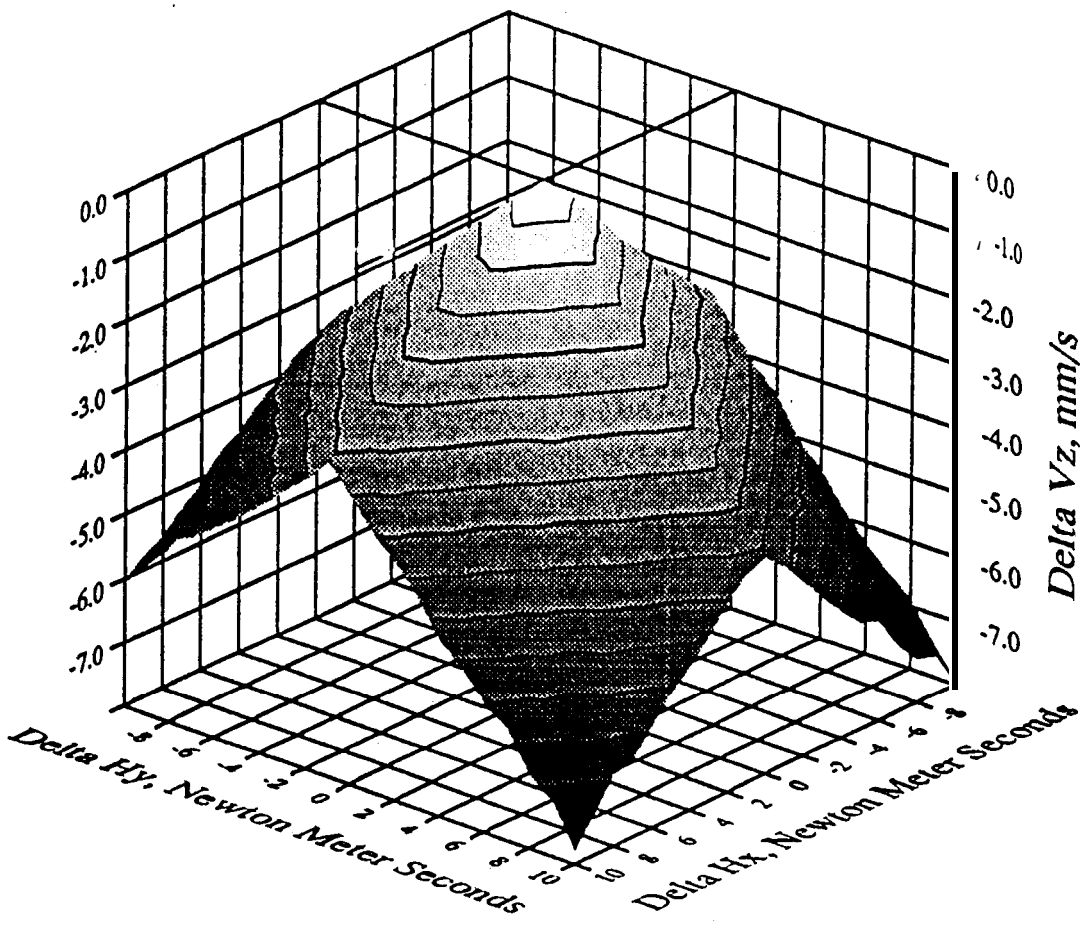

Figure 5: 3D contour plots of V_z versus (H_{wx}, H_{wy}) for EOM conditions

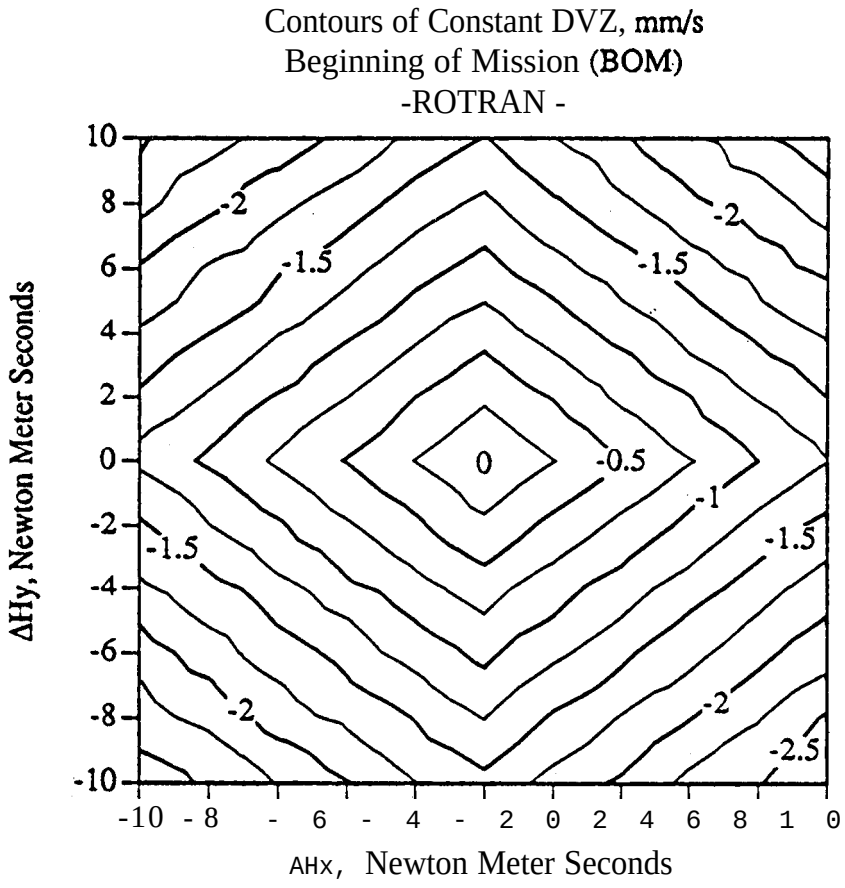

Figure 6: 2D contour plots of V_z versus (H_{wx}, H_{wy}) for *BOM* conditions

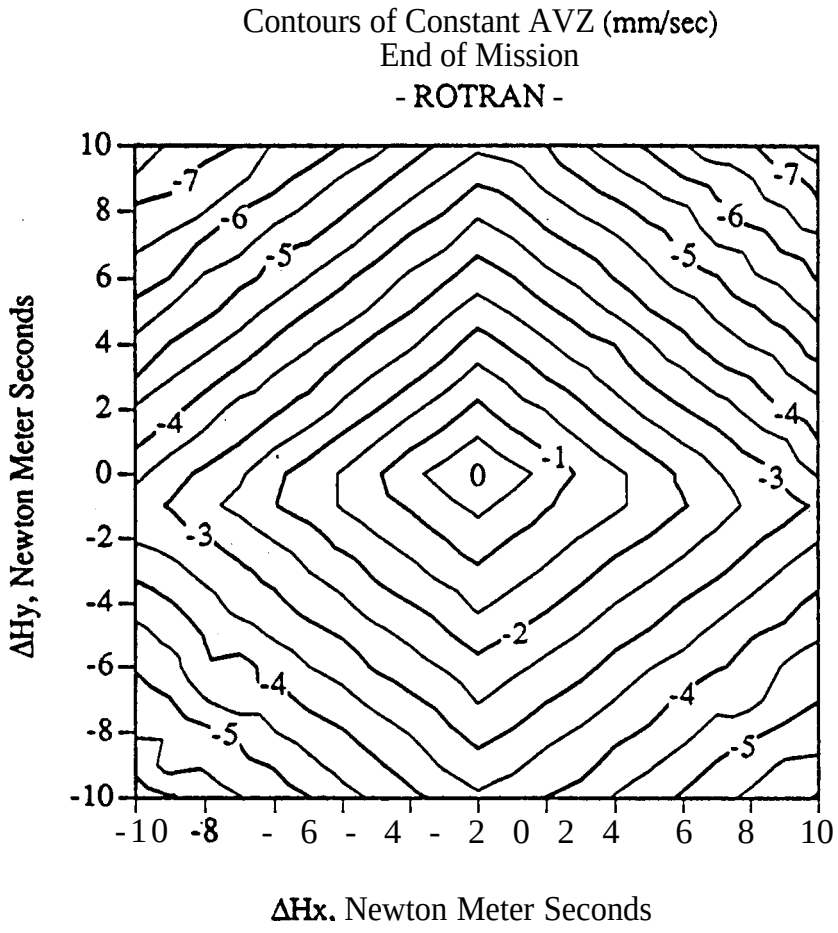

Figure 7: 2D contour plots of V_z versus (H_{wx}, H_{wy}) for EOM conditions

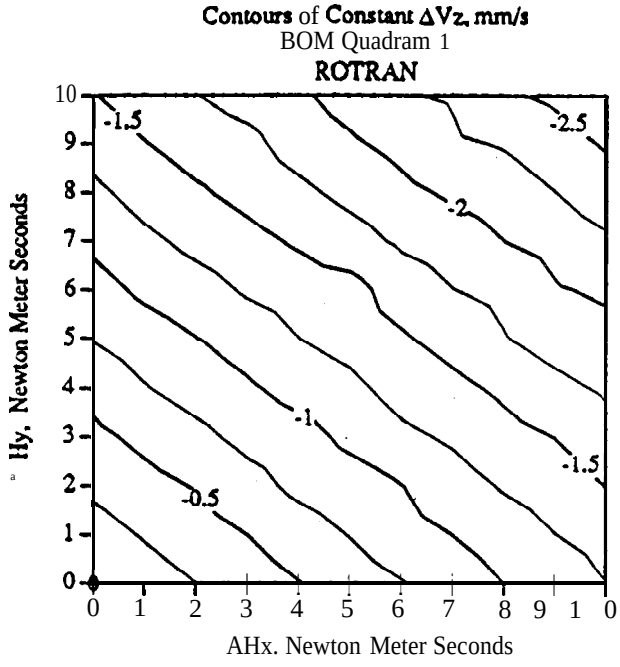

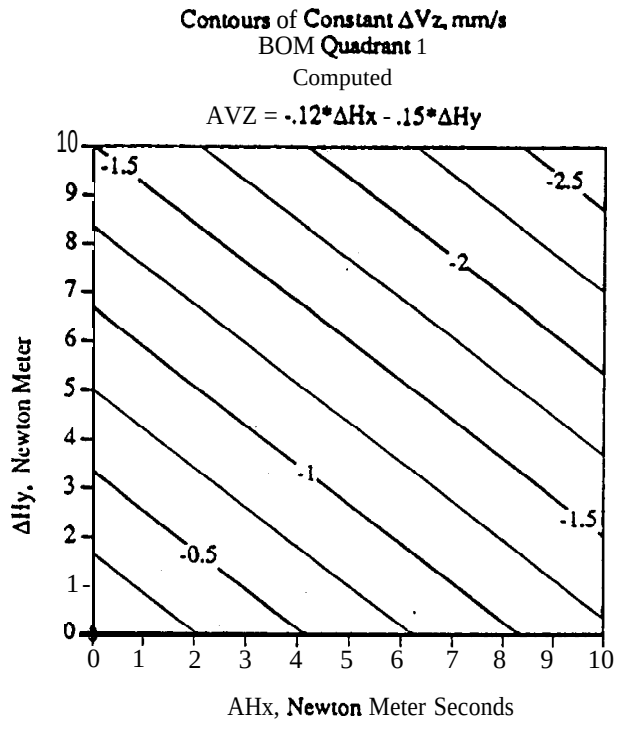

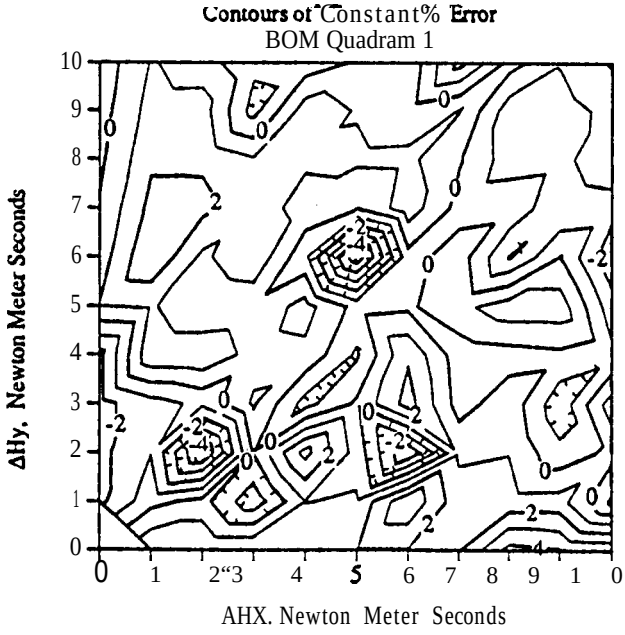

Figure 8: Linear approximation results - (BOM, quadrant 1)

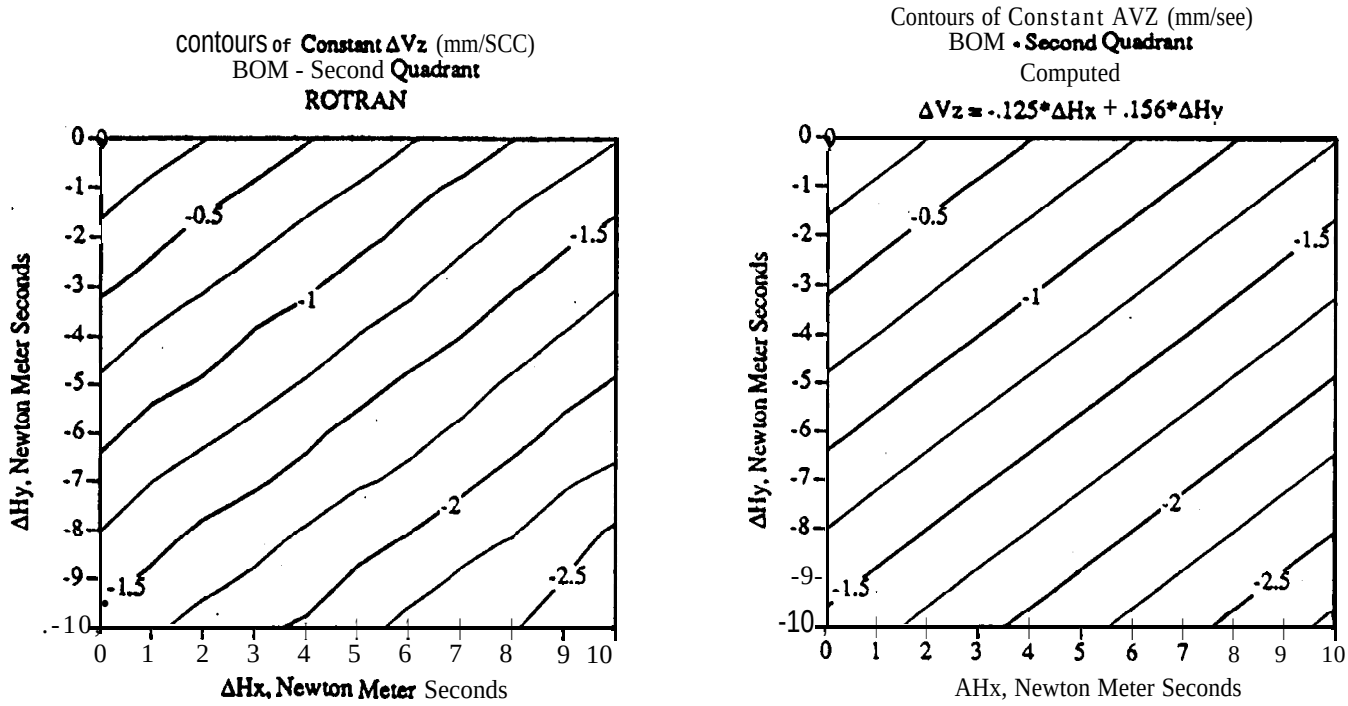

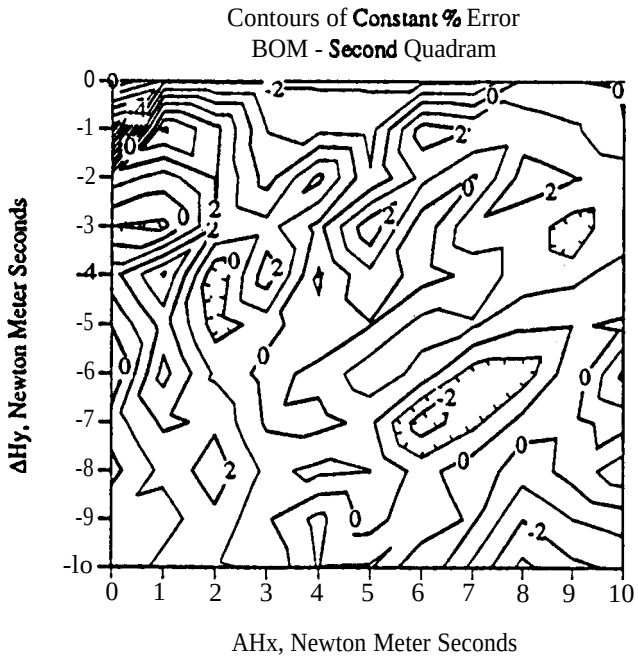

Figure 9: Linear approximation results - (BOM, quadrant 2)

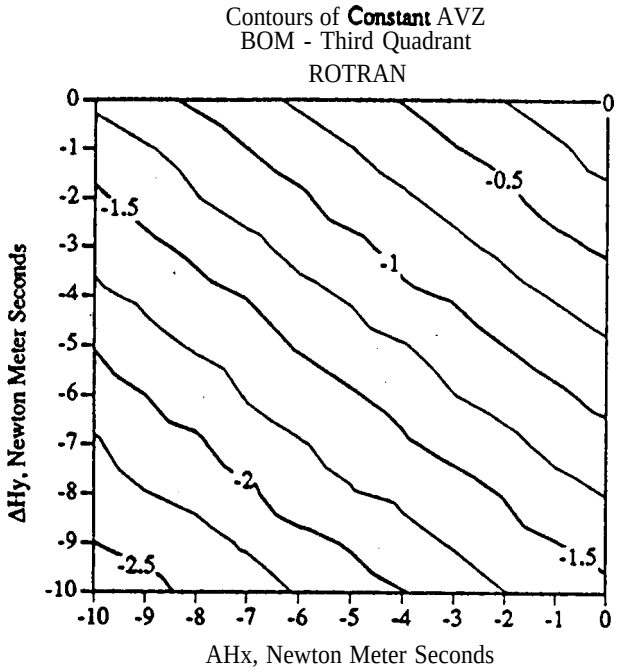

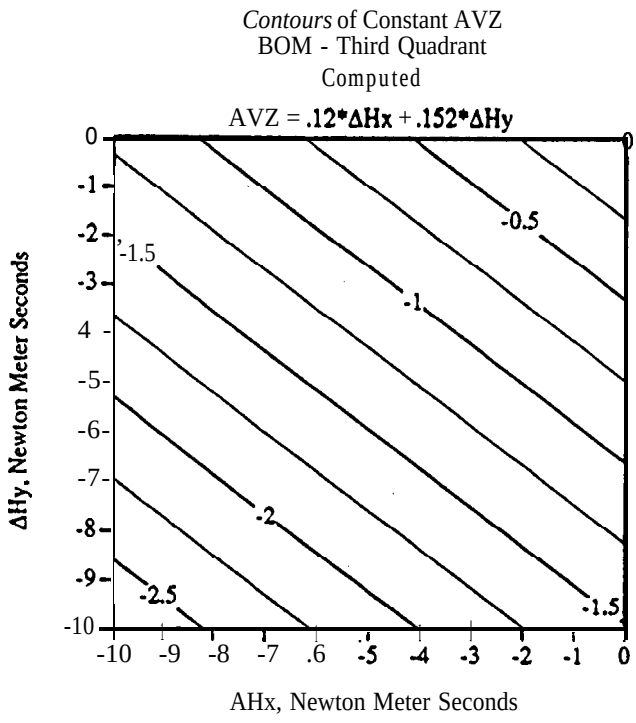

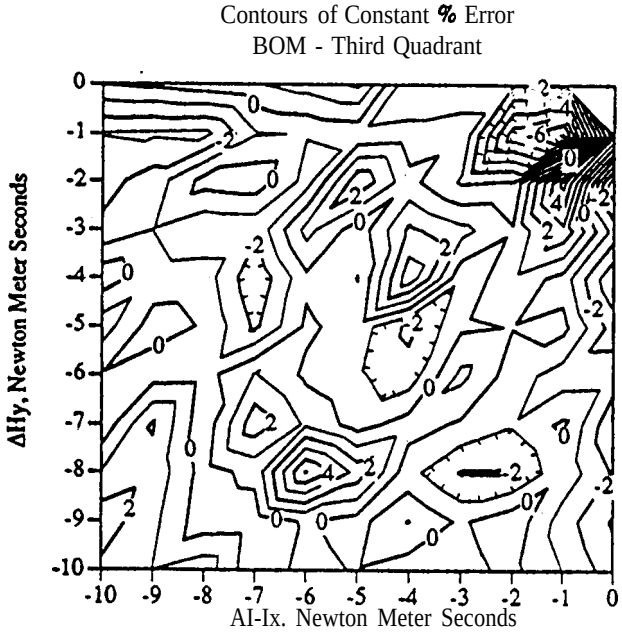

Fig;ure 10: Linear approximation results - (BOM, quadrant 3)

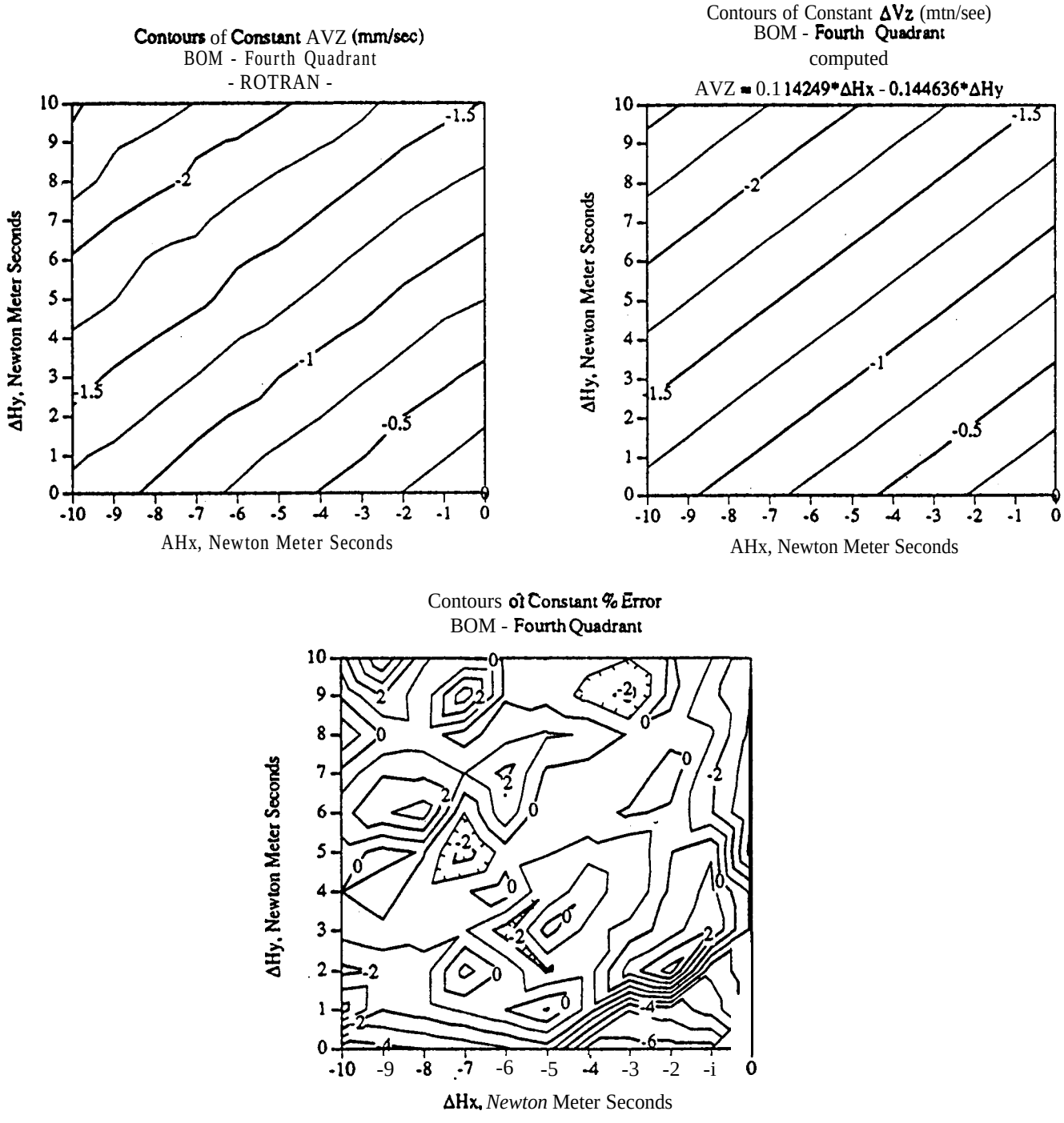

Figure 11: Linear approximation results - (BOM, quadrant 4)

Contours of Constant AVZ (mm/sec)
End of Mission -First Quadrant
-ROTRAN -

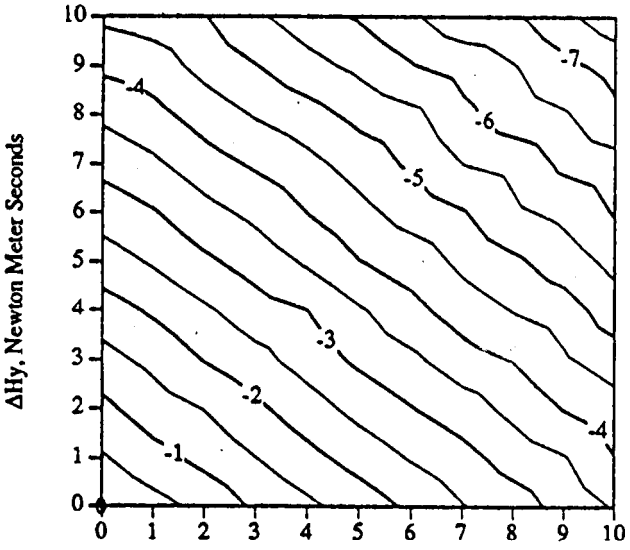

Contours of Constant AVZ (mm/see)
End of Mission -First Quadrant
Computed
AVZ = -.34018 *AHx. .437198*ΔHy

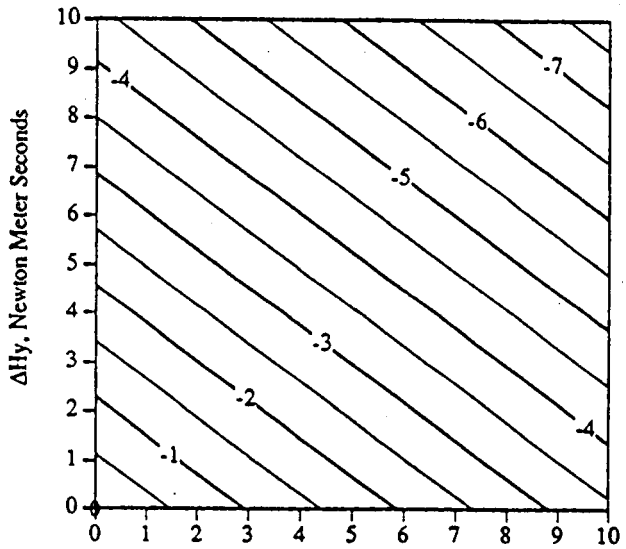

Contours of Constant% Error
End of Mission - First Quadrant

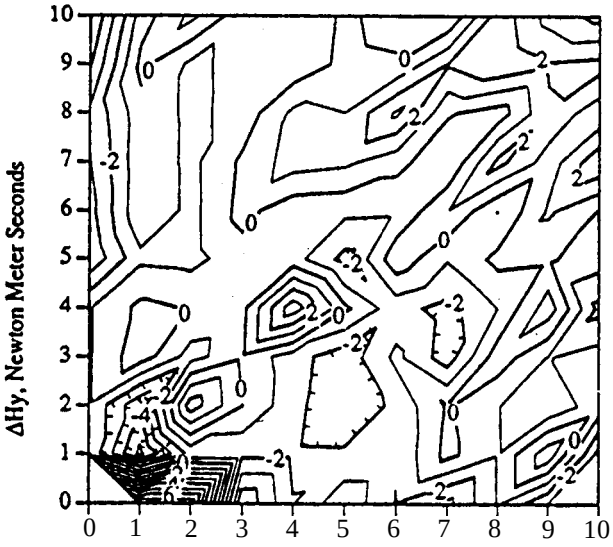

Figure 12: Linear approximation results - (EOM, quadrant 1)

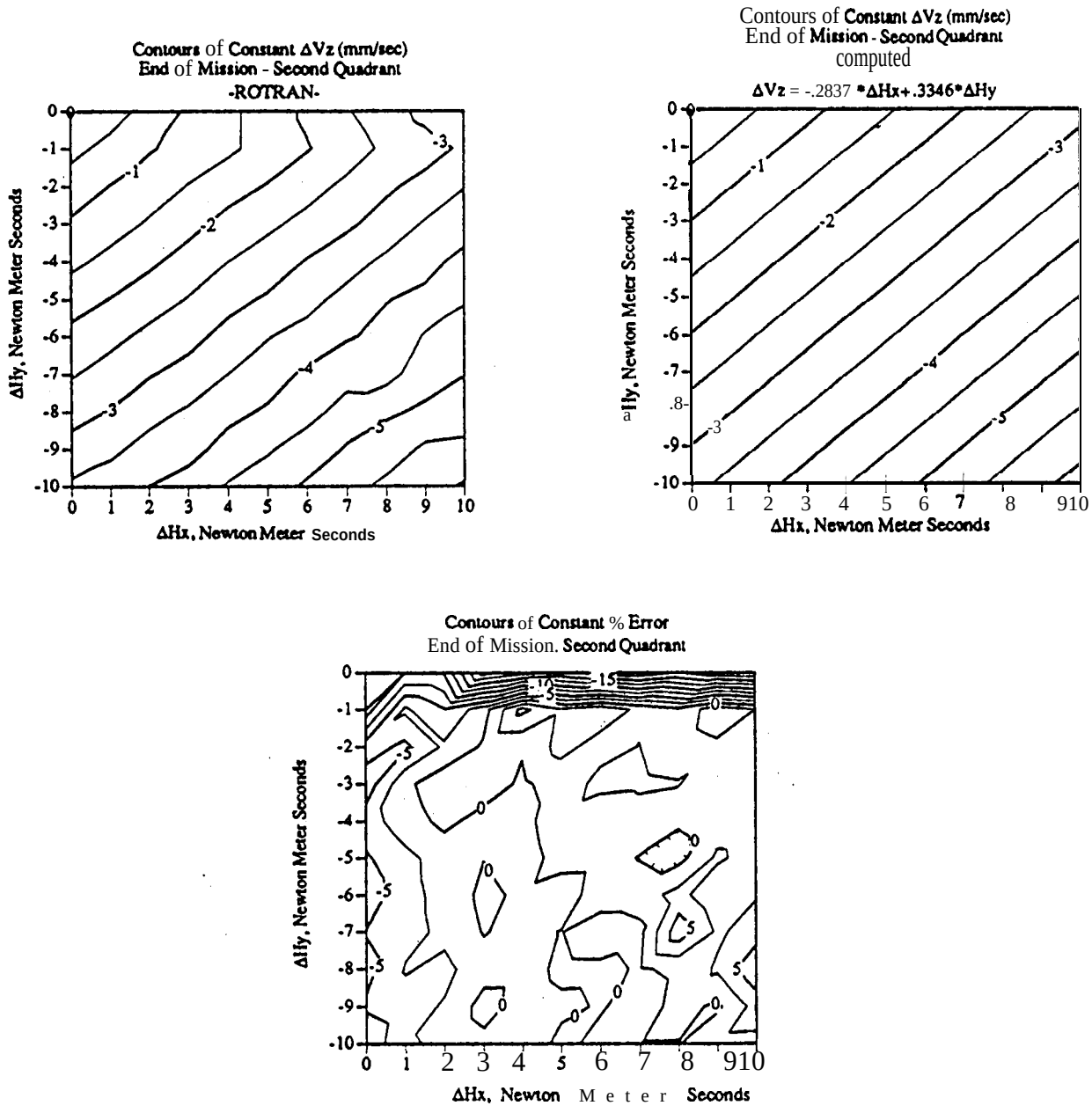

Figure 13: Linear approximation results - (EOM, quadrant 2)

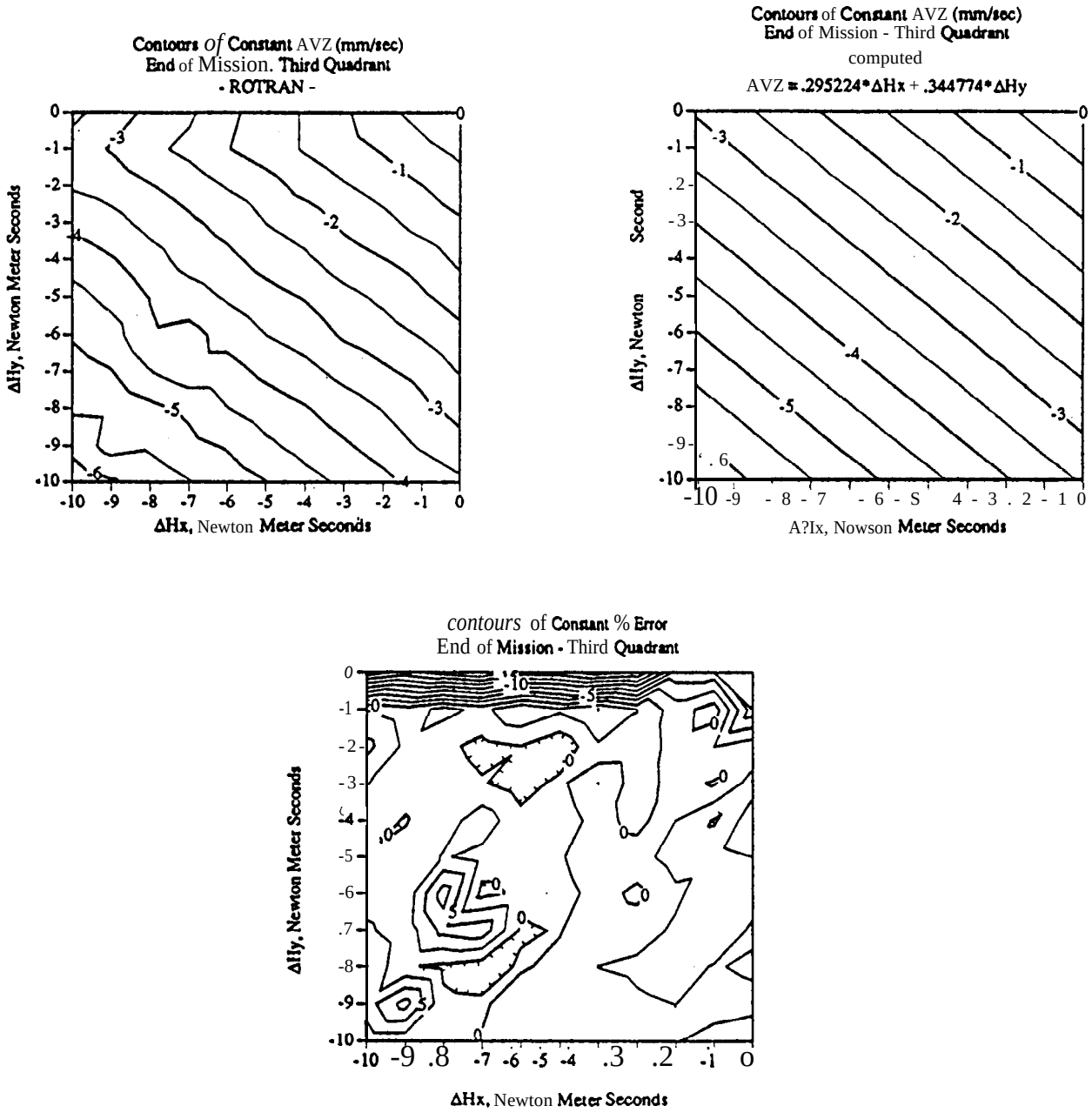

Figure 14: Linear approximation results - (EOM, quadrant 3)

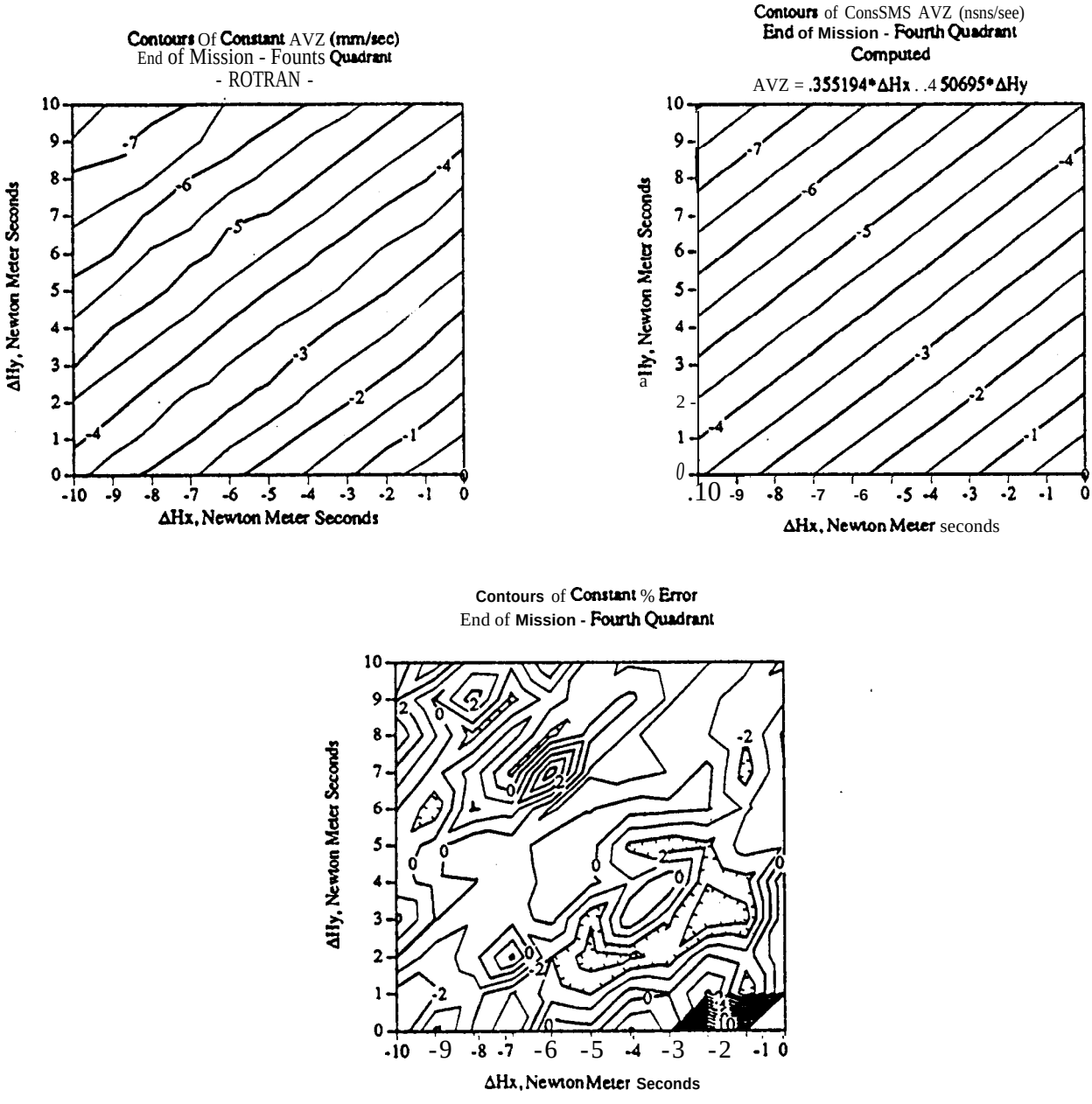

Figure 15: Linear approximation results - (EOM, quadrant 4)

Quadrant	Coefficients ($\frac{mm}{KgM^2}$)	
	BOM	EOM
$(+x,+y)$	$(-0.12,-0.15)$	(-0.34018, -0.437198)
$(+x,$ -Y)	(-0.125,0.156)	(-0.2837,0.3346)
(-x, -y)	(0.12,0.152)	(0.295224, 0.344774)
$(-x,+y)$	(0.114249,-0.144636)	(0.355194, -0.450695)

Table 6: Linear coefficients for each quadrant, HOM and EOM

4 Conclusions

$\Delta\vec{\mathbf{V}}_{cm}$ is independent of N_{wz} to within about 4% at worst as shown in Tables (3) and (4). The linear approximation of Eq. (6) is valid with a dominant 4% to 10'% error as can be seen in Figs. (8) thru (15). Acceptance of this approximation eliminates the need to use the full power of *ROTRAN* to generate $\Delta\vec{\mathbf{V}}_{cm}$ except for an initial generation of runs needed for the pseudo-inverse of Eq. (10).

Note that the coefficients $\mathbf{C_i}$ depend on mass properties, thruster configurations, the control law, etc. If any of these change, then new coefficients will have to be generated accordingly,

Table (6) summarizes the coefficients.

References

[1] Sengsta.eke, Marc A., *ROTRAN - Theory And Implementation In Software, Revision 1,* California Institute of Technology, Jet Propulsion Laboratory, Engineering Memorandum # 314-554, March 1993

[2] Sengstacke, Marc A., *ROTRAN Documentation Update #1,* California Institute of l'ethnology, Jet Propulsion Laboratory, Engineering Memorandum # 314-571, September 1993

[3] Lee, Larry W., *Cassini Project, Project Mass Properties Report, Issue #1,* Sept. 11, 1992, PD 699-013, California Institute of Technology, Jet Propulsion Laboratory